Journal of Flood Risk Management

WILEY

CIWEM Chartered Institution of Water and Environmental Management | Journal of Flood Risk Management

SPECIAL ISSUE PAPER | OPEN ACCESS

Bridge Collapse in Mutsu, Aomori Prefecture, Japan in 2021

Hiroshi Takebayashi | Masaharu Fujita

Disaster Prevention Research Institute, Kyoto University, Kyoto, Japan

Correspondence: Hiroshi Takebayashi (takebayashi.hiroshi.6s@kyoto-u.ac.jp)

Received: 1 October 2023 | **Revised:** 30 July 2024 | **Accepted:** 23 November 2024

Funding: This work was supported by Ministry of Land, Infrastructure, Transport and Tourism, Japan.

Keywords: bank erosion | bed deformation | bridge collapse | bypassing flow | field survey | numerical simulation

ABSTRACT

On August 9–10, 2021, the Koakagawa Bridge in Mutsu, Aomori Prefecture, Japan, collapsed owing to the flood caused by a tropical cyclone. In this study, the cause of the collapse was examined. The characteristics of flood inundation with bypassing flows and countermeasures for bank erosion due to channel blockage by driftwood were investigated based on field surveys and numerical simulations. The scouring of the bed around the bridge pier was found to be the cause leading to bridge failure. Channel blockage owing to driftwood would have caused flood inundation and damage to the left bank, the top of the bank is bare of sediment, by forming a bypassing flow. However, the surface of the right bank on which the bypassing flow with high velocity formed was covered with concrete; therefore, bank erosion did not occur. These results indicate that to prevent bank erosion caused by bypassing flows during floods, it is important to protect banks downstream of the bridge using non-erosive materials. Only a small area, where bypassing flows form and non-dimensional shear stress is larger than 0.05, is sufficient for protection. It is also important to predict bed degradation characteristics around piers and banks, especially when the bed material is small.

1 | Introduction

From August 9 to 10, 2021, torrential rain caused by a tropical cyclone formed by Typhoon Lupit caused many slope failures and debris flows in the northern Shimokita Peninsula in Aomori Prefecture in Japan. No human casualties were reported, but road traffic was blocked, and many residents were isolated owing to the destruction of bridges and the flooding of roads with sediment. In the Koakagawa River Basin (Figure 1) located in Ohata in Mutsu City, Aomori Prefecture, Japan, slope failures and debris flows produced a large amount of driftwood that was transported along with floodwater and sediment into the lower reaches of the Koakagawa River. Driftwood flowing down the Koakagawa River accumulated at the Koakagawa Bridge and blocked the river channel.

When slope failures and debris flows occur during heavy rainfall, trees on the slopes become driftwood, supplied to the river channel and transported downstream by floods and debris flows. This phenomenon is frequently observed in watersheds with steep slopes. Driftwood flowing down the river channel accumulates in areas with small river cross-sections, such as bridges with piers, thus causing channel blockages that contribute to flood inundation and increase the stresses that destroy buildings when they collide with them during inundation (Diehl 1997; Fischer 2006; Lyn et al. 2007; Ruiz-Villanueva, Bodoque, et al. 2014; Lucía et al. 2015; Comiti et al. 2016; Okamoto et al. 2016). In addition, the inundation area of a flood with driftwood may differ considerably from that of a flood without driftwood.

The transport of driftwood, which causes channel blockage, and the processes of production, transport, and deposition of driftwood have been studied using physical models and flume experiments (Braudrick and Grant 2000; May and Gresswell 2003; Bragg and Kershner 2004; Mazzorana et al. 2010). Braudrick and Grant (2001) conducted flume experiments to examine the transport and deposition of driftwood by floodwater. Lyn et al. (2003) investigated the effects of flow velocity and water depth on the rate of channel blockage by driftwood. Bocchila et al. (2006) showed that the probability of channel blockage due to driftwood depends on the length of the driftwood and the flow regime. Bocchila et al. (2008) statistically examined the relationship between channel blockage (due to driftwood) and the transport distance of driftwood. Wohl and Jaeger (2009) investigated the relationship between the hydraulic parameters and channel blockage caused by driftwood. Schmocker and Hager (2011) showed that the rate of channel blockage by driftwood increased with increasing water depth and decreased with increasing Froude numbers. Ruiz-Villanueva, Bladé, et al. (2014) developed a two-dimensional model to reproduce the transport and deposition processes of driftwood, and the model reproduced changes in water level and velocity due to driftwood deposition. In addition, empirical equations have been proposed to predict the rate of channel blockage by driftwood in river structures, such as bridges and weirs. Schalko (2017) found that the rate of channel blockage by driftwood increased as a function of the length of the driftwood and with a slow approach velocity. They also showed that the Froude number had little effect on the channel blockage rate. De Cicco et al. (2018) reviewed the factors that affected channel blockage by driftwood at bridge piers. Driftwood not only causes flooding but also poses many problems such as post-disaster disposal. Le Lay and Moulin (2007) have investigated these issues.

Several studies have been conducted on water-level rise due to driftwood accumulation at bridges. Schmocker and Hager (2013) and Schalko et al. (2018) conducted driftwood accumulation experiments and examined the governing parameters of the Froude number in the approaching flow from upstream and the length of the driftwood accumulation zone. They showed that the water level in the backwater increased as the Froude number in the approaching flow and the length of the driftwood accumulation zone increased. They also showed that the water level of the backwater increased as the driftwood diameter decreased. Panici and de Almeida (2018) investigated the occurrence and development of driftwood accumulation at bridge piers and found that the flow regime and length of the driftwood accumulation area strongly depended on the length of the flow in that area.

Most of the existing studies on driftwood have been limited to the examination of in-channel phenomena. Suppressions of both the accumulation of driftwood and the increase in water levels of backwater due to the overflow of water and driftwood from a river to floodplains have not been considered. Consequently,

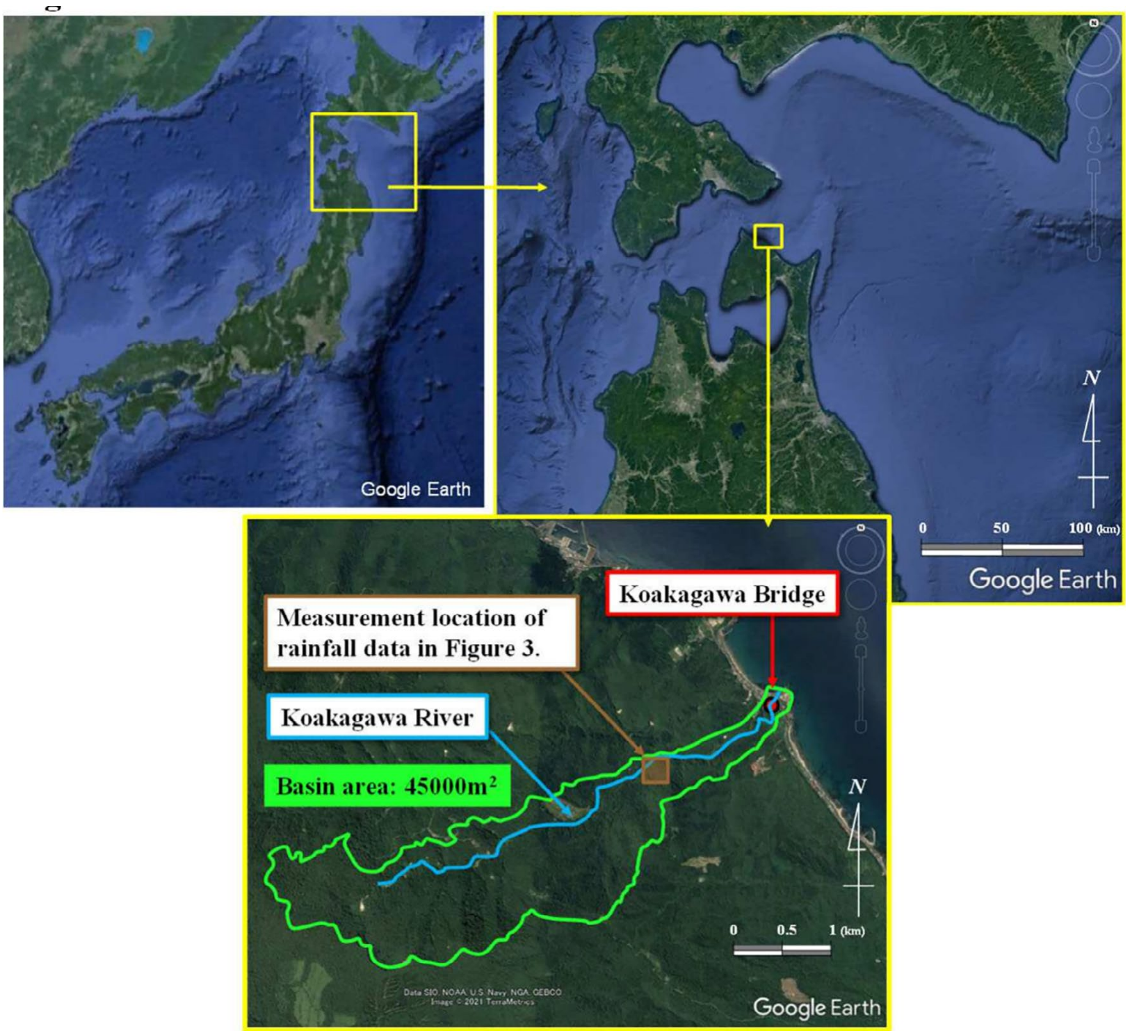

FIGURE 1 | Location of Koakagawa River Basin.

evaluations were pursued considering the water level of the backwater to be high.

In an actual river, the rise of the water level in the upstream area owing to driftwood accumulation at bridges causes overflows, which in turn cause house runoffs and ground erosion in the floodplain around bridges. Okamoto et al. (2020) conducted experiments considering the floodplains and found that the velocity distribution on a floodplain is useful for estimating the location of ground erosion damage due to flood flow. In a non-leveed river channel, inundated floodwater forms bypassing flows that return to the river channel downstream of the bridge. At the point at which the bypassing flows return to the channel, water flows into the channel from the top of the bank on the steep slope, and the banks are easily eroded. Therefore, there is an urgent need to clarify the characteristics of bypassing flows and countermeasures. However, the aforementioned studies have not focused on the characteristics of bypassing flows—from the top of the bank to the river channel—that have the greatest effects on bank erosion.

This study examined the cause of the collapse of the Koakagawa Bridge in Mutsu City in the Aomori Prefecture in Japan. The characteristics of flood inundation with bypassing flows and countermeasures for bank erosion owing to channel blockage by driftwood were investigated based on field surveys and numerical simulations of horizontal two-dimensional bed deformation.

2 | Disaster Characteristics Occurred in the Koakagawa River Basin

2.1 | Koakagawa River Basin

The Koakagawa River Basin is located in the north of Honsyu Island in Japan, as shown in Figure 1. Figure 2a shows land elevation in and around the Koakagawa River Basin. The higher ground elevation is located in the western part of the river basin, at the highest elevation of approximately 800 m. The Koakagawa River flows westward into the Tsugaru Straits. The length of the main channel of the Koakagawa River is 6 km. The river basin area of the river is 45,000 m^2. Figure 2b shows the geological conditions in and around the Koakagawa River Basin. The prevailing geological conditions feature rock formations such as Dacite and Rhyolite. The geological condition in the higher land elevation area comprises Andesite. The Koakagawa River Basin is managed by Aomori Prefecture, which is the local government. According to the Köppen climate classification chart (Köppen 1936), the basin is located in a Dfb climate region (Cold, no dry season, warm summer). The annual average atmospheric temperature is 9.5°C, and the annual accumulated rainfall is 1342 mm.

2.2 | Rainfall Characteristics

In this study, rainfall intensity data from X-band and C-band mixed radar were utilized. The target location was measured by two radars: one from the north and the other from the south. Notably, the attenuation of rainfall intensity from radar measurements in the north is negligible owing to the sea area north of the target site, which offers no obstruction to the radar. As illustrated in Figure 4, the high rainfall intensity area is extremely narrow, and there are no rainfall measurement points by rain gauges within the same rainfall area as the target river basin.

Figure 3 presents the temporal variation in rainfall intensity measured in the brown square area in Figure 1, as obtained by the mixed C-band/X-band radar. Rainfall commenced at approximately 11:00 a.m. on August 9 and continued intermittently until 3:00 p.m. on August 10. Following a period of low-intensity rainfall from 11:00 p.m. on August 9 to 2:00 a.m. on August 10, rainfall intensity increased again, achieving a maximum intensity of 74 mm/h. Driftwood obstructed the

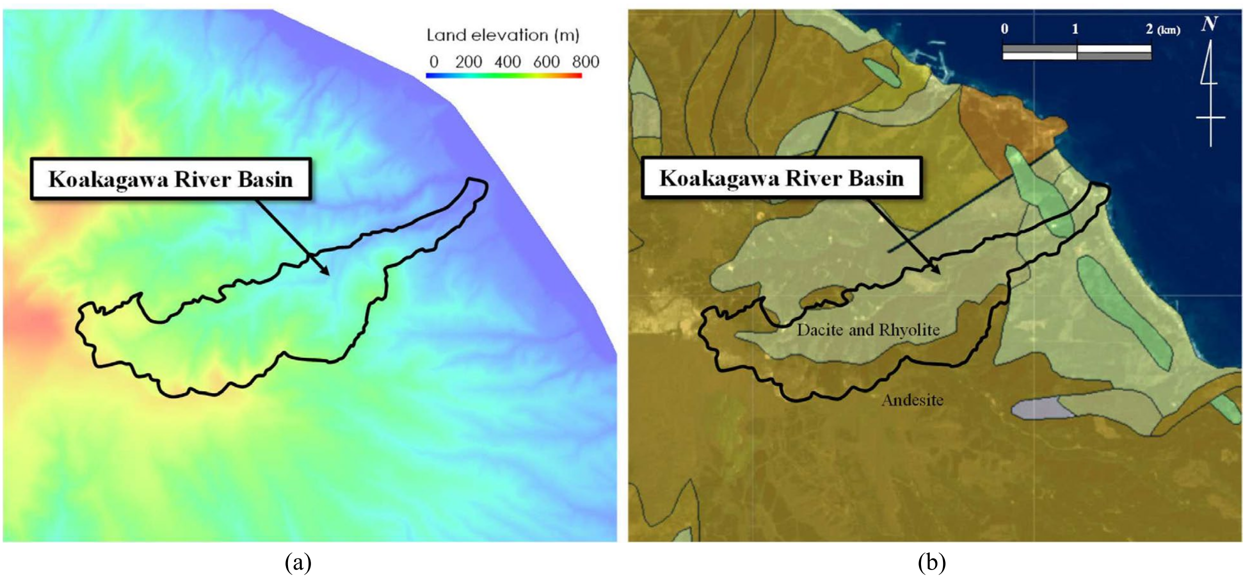

FIGURE 2 | Land elevation and geological condition in and around Koakagawa River Basin. (a) Land elevation (Geospatial Information Authority of Japan) (b) Geological condition (National Institute of Advanced Industrial Science and Technology).

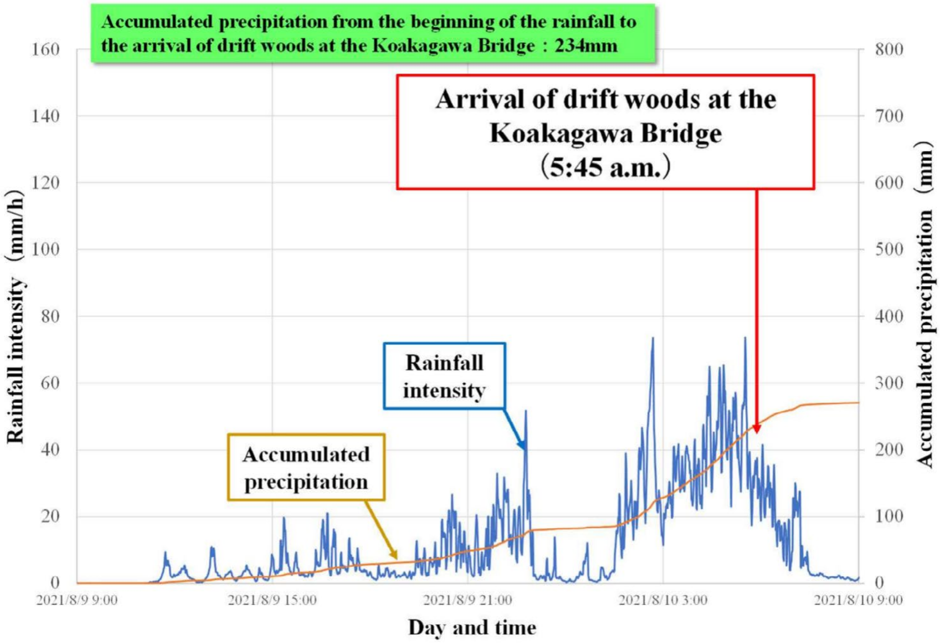

FIGURE 3 | Temporal change of rainfall intensity in the upper reach of the Koakagawa River in Ohata-cho, Mutsu City, obtained from C-band/X-band mixed radar.

river channel at approximately 5:45 a.m. on August 10, and despite the rainfall intensity having peaked, the rainfall remained strong at 32 mm/h. The rainfall accumulated from the beginning of the rainfall until 5:45 a.m. on August 10 was 235 mm, according to the mixed C-/X-band radar rainfall data. Thus, slope failures and debris flows can occur with relatively small total precipitation.

Figure 4 depicts the spatiotemporal changes in sediment disaster risk obtained using a real-time sediment disaster risk assessment system (Igarashi et al. 2016). The figure also shows the spatial distribution of rainfall intensity obtained by the mixed C-band/X-band radar. The sediment disaster risk was calculated using land slope, rainfall intensity per minute, and other relevant factors. The horizontal resolution of the risk indication was 250 m × 250 m.

The wind blew from the south-southeast owing to the tropical cyclone. Consequently, as indicated by the distribution of rainfall intensity at 11:00 p.m. on August 9 and 5:00 a.m. on August 10, a stationary line-shaped precipitation system extending from east of Mt. Osore formed, resulting in continuous heavy rainfall in the same location. The sediment disaster risk level in Ohata-cho, Mutsu City, began to increase at approximately 3:00 a.m. on August 10 and reached a high-risk level of 4 at approximately 6:00 a.m., when the driftwood generated by the slope failures and debris flows was transported to the Koakagawa Bridge. These results indicate that although the total precipitation amount was relatively small, the short but high-intensity rainfall from the stationary line-shaped precipitation system caused slope failures and debris flows. The sediment disaster risk level decreased over time, and by approximately 8:10 a.m., there was no indication of sediment disaster risk levels.

2.3 | Collapse of Koakagawa Bridge and Flood Inundation

Figure 5 shows the Koakagawa Bridge and its surroundings after the disaster. Figure 6 shows the geometric characteristics of the collapsed bridge. A pier is located at the center of the bridge. Figure 5a shows that a large amount of driftwood accumulated upstream of the Koakagawa Bridge and that floodwaters containing sediments inundated the area around the Koakagawa River. Figure 7 shows the inundated area on the left bank of the Koakagawa River after the disaster. The thickness of the deposited sediment was 1.2 m, and the average grain size of the inundated sediment was 2 mm, indicating that a large amount of fine sediment was inundated (see Figure 8).

Figure 5a illustrates that the Koakagawa Bridge has a pedestrian sidewalk upstream and a roadway downstream, with only the roadway part collapsing. The left bank of the bridge fell into the riverbed, while the right bank girder remained on its bearing, indicating that the bridge failure was strongly influenced by erosion on the left bank. Additionally, the intact pedestrian sidewalk suggests that the collapse was not caused by the impact of driftwood. By contrast, driftwood accumulated on the Koakagawa Bridge, blocking the river channel and causing a bypassing flow from the top of the levee to the river channel downstream of the bridge. This detour eroded the bank and led to the bridge's collapse. Furthermore, due to the curved horizontal shape of the river channel around the bridge section, the flow was concentrated on the left bank, which is the outer bank of the curve, resulting in bank collapse due to local scouring. Figure 5b shows that the bridge piers located in the center of the river channel subsided, indicating that scouring of the bed around the pier contributed to the bridge failure.

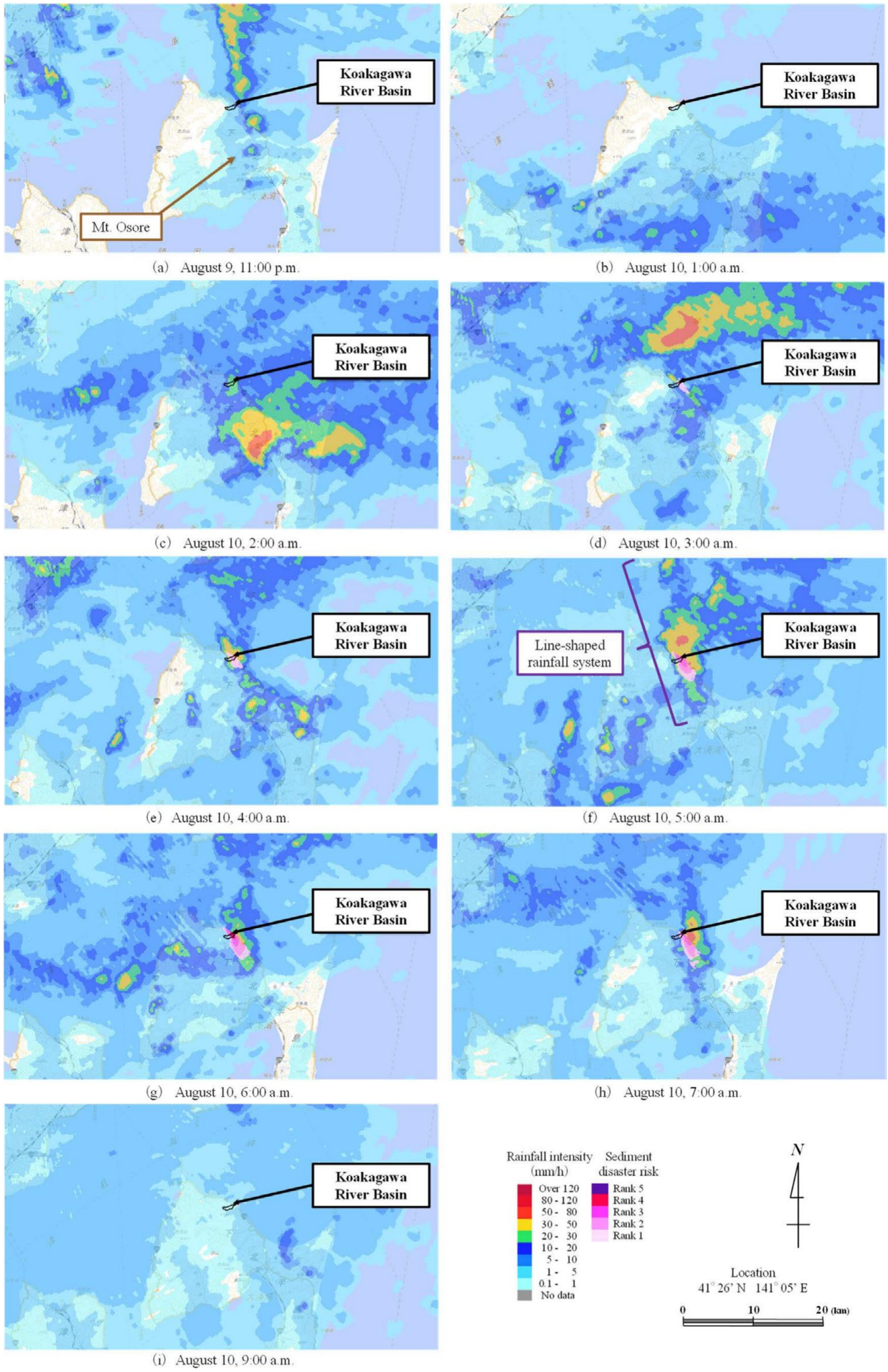

FIGURE 4 | Spatiotemporal changes in the sediment disaster risk and rainfall intensity obtained using the real-time sediment disaster risk assessment system (Igarashi et al. 2016) (Background image: GSI).

Figure 9 shows the Koakagawa Bridge captured at approximately 5:00 a.m. on August 10. Figure 9 shows that the pier subsided by approximately 1 m. At this point, the subsidence of the pier was not very deep, and the left bank of the bridge girder was on the bearing. Figure 10 shows the abutment of the bridge girder at the top of the pier after the disaster. In other words, the pier subsided almost vertically by approximately 3 m. The bed material around the pier was composed of small sediments with a grain size of 5 mm, as shown in Figure 10. As shown in Figure 9, at approximately 5:00 a.m. on August 10, driftwood did not accumulate upstream of the bridge, and no flood inundation occurred. In other words, the driftwood did not affect the initiation of bridge failure. The situation in Figure 9 differs from that in Figure 5a, and additional phenomena, including driftwood accumulation, are considered to have caused the complete bridge failure and flood inundation. These phenomena are discussed using numerical simulations.

(a)

(b)

FIGURE 5 | Flood inundation and collapse of the Koakagawa Bridge. (a) Koakagawa bridge and inundation area (photo: Asia Air Survey Co. Ltd.) (b) Collapse of the bridge pier (photo: Aomori Prefecture).

2.4 | Sediment and Driftwood Production in the Koakagawa River Basin

Figure 11 presents the Koakagawa River watershed after the disaster. As shown in Figure 11c, several slope failures occurred. In addition, traces of debris flows can be observed on the right-hand side of Figure 11b. Furthermore, as shown in Figure 11a, several large-scale slope failures occurred, which are the sources of sediment and driftwood around the Koakagawa Bridge. As shown in Figure 11d,f, sabo dams were installed in the river, but they were all full of sediment, indicating that it was difficult to capture most of the driftwood. Figure 11h shows the land deformation before and after the disaster. It can be seen that sediments eroded by slopes are deposited into the river channel in large quantities. The two sabo dams could not stop these sediments, and they are transported downstream. However, the bed has been degraded in the vicinity of the bridge.

3 | Numerical Simulations of Flow and Bed Deformation Around the Koakagawa Bridge

3.1 | Basic Equations

The basic equations used in the numerical simulations are based on a horizontal two-dimensional bed deformation analysis model (Takebayashi 2017) with a general coordinate system. The numerical analysis model was implemented in the application software iRIC, which was developed by a research group

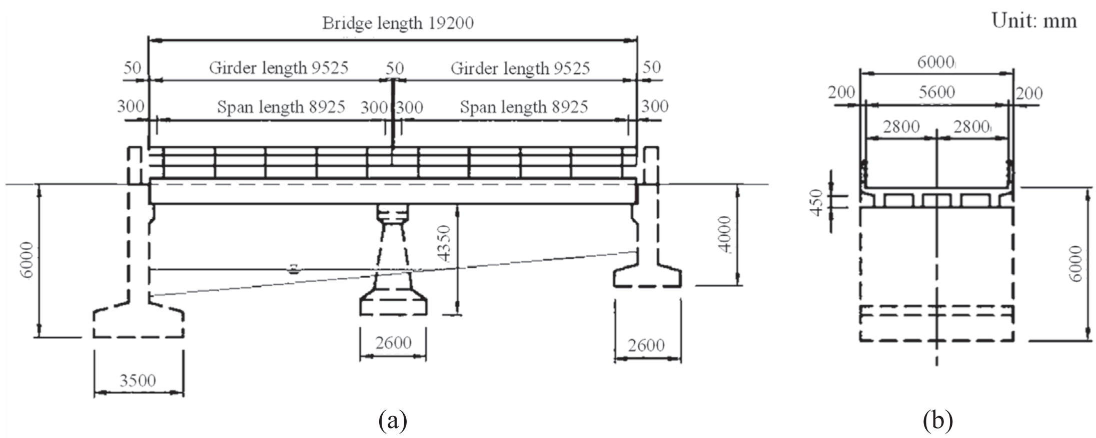

FIGURE 6 | Geometric characteristics of the Koakagawa bridge (Aomori Prefecture). (a) Side view. (b) Cross-section view.

FIGURE 7 | Sediment deposition in the inundation area.

FIGURE 8 | Koakagawa bridge at 5:00 a.m. on August 10 (photo: Aomori Prefecture).

FIGURE 9 | Abutment of the bridge girder at the top of the pier (photo: Aomori Prefecture).

FIGURE 10 | Bed material in the Koakagawa River near the Koakagawa Bridge.

including the first author (Nelson et al. 2016). In the simulation of the flow and bed deformation around the Koakagawa Bridge, the bed material was treated as non-cohesive with a uniform grain size. The bed load was considered to reproduce the bed deformation process. The equations used in the numerical analysis are as follows.

The relationship between a Cartesian coordinate system and a generalized curvilinear coordinate system is given as follows:

$$J = \frac{1}{\left(\frac{\partial x}{\partial \xi}\frac{\partial y}{\partial \eta} - \frac{\partial x}{\partial \eta}\frac{\partial y}{\partial \xi}\right)} \tag{1a}$$

$$\frac{\partial \xi}{\partial x} = J\frac{\partial y}{\partial \eta} \tag{1b}$$

$$\frac{\partial \eta}{\partial x} = -J\frac{\partial y}{\partial \xi} \tag{1c}$$

$$\frac{\partial \xi}{\partial y} = -J\frac{\partial x}{\partial \eta} \tag{1d}$$

$$\frac{\partial \eta}{\partial y} = J\frac{\partial x}{\partial \xi} \tag{1e}$$

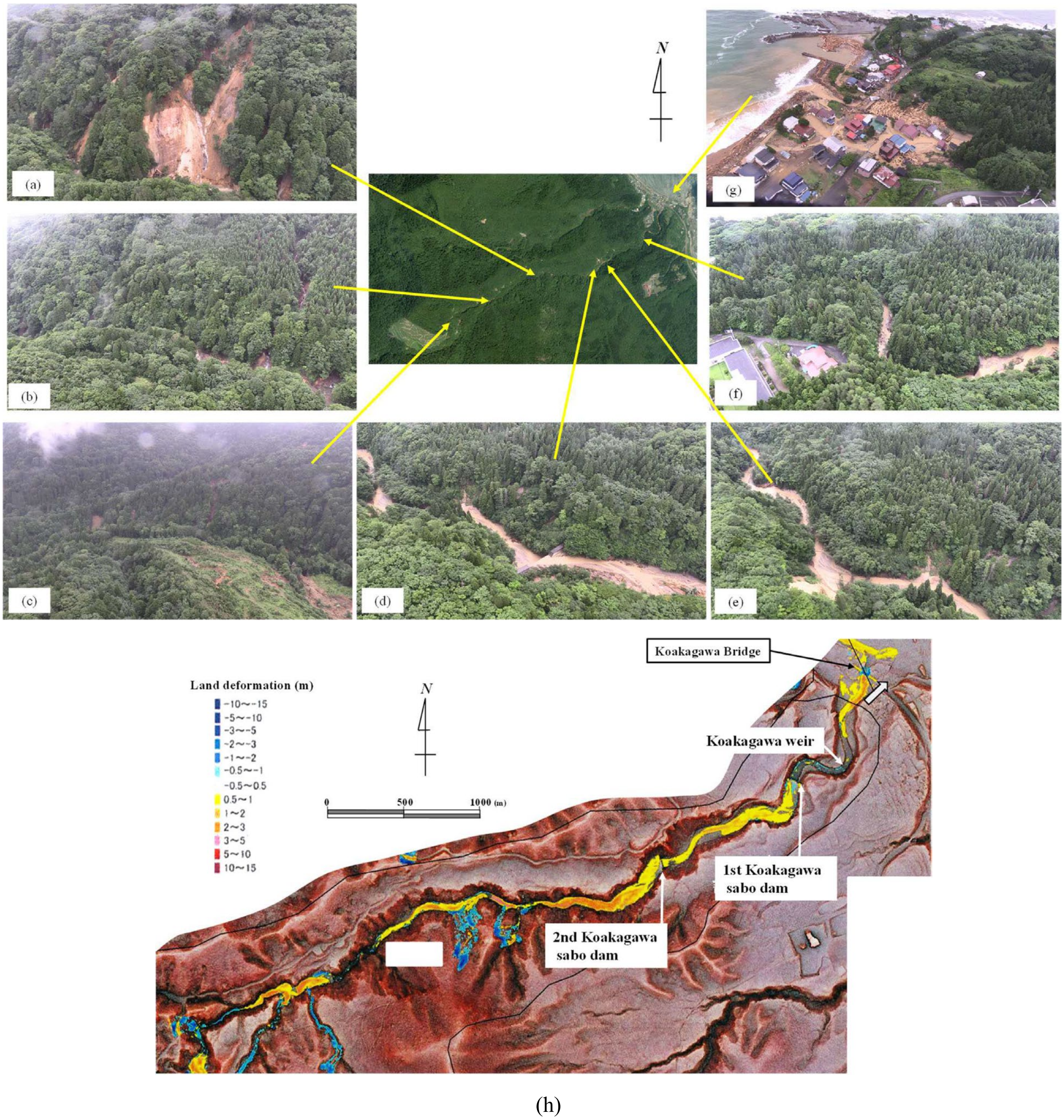

FIGURE 11 | Production of driftwood and sediment in the Koakagawa River basin (photos are taken by Aomori Prefecture's disaster-prevention helicopter "Shirakami" on August 12) and land deformation before and after the disaster (Aomori Prefecture).

where ξ and η are the coordinates along the longitudinal and transverse directions in a generalized curvilinear coordinate system, respectively, and x and y are the coordinates in a Cartesian coordinate system.

The surface flow is calculated using the governing equation for horizontal two-dimensional flow averaged over depth. Groundwater is modeled as a horizontal two-dimensional saturation flow. The surface of driftwood accumulation is treated as the bed surface, and the water flow within the driftwood accumulation is treated as groundwater. The exchange of momentum between surface water and groundwater flow is not considered; only mass exchange between them is considered. The conservation of mass, including the inflow and outflow of mass by seepage flow, is taken into account as shown in the following equation (Takebayashi 2017).

$$\Lambda\frac{\partial}{\partial t}\left(\frac{z}{J}\right)+\frac{\partial}{\partial \xi}\left(\frac{hU}{J}\right)+\frac{\partial}{\partial \eta}\left(\frac{hV}{J}\right)+\frac{\partial}{\partial \xi}\left(\frac{h_g U_g}{J}\right)+\frac{\partial}{\partial \eta}\left(\frac{h_g V_g}{J}\right)=0 \quad (2)$$

where t is the time, and z is the water surface level. Surface flow depth is represented as h, and seepage flow depth is h_g. U and

V represent the contravariant depth-averaged flow velocities above the bed along the ξ and η coordinates, respectively.

These velocities are defined as

$$U = \frac{\partial \xi}{\partial x} u + \frac{\partial \xi}{\partial y} v \tag{3}$$

$$V = \frac{\partial \eta}{\partial x} u + \frac{\partial \eta}{\partial y} v \tag{4}$$

where u and v represent depth-averaged flow velocities above the bed along the x and y coordinates, respectively. U_g and V_g represent the contravariant depth-averaged seepage flow velocities along the ξ and η coordinates, respectively. These velocities are defined as

$$U_g = \frac{\partial \xi}{\partial x} u_g + \frac{\partial \xi}{\partial y} v_g \tag{5}$$

$$V_g = \frac{\partial \eta}{\partial x} u_g + \frac{\partial \eta}{\partial y} v_g \tag{6}$$

where depth-averaged seepage flow velocities along x and y coordinates in a Cartesian coordinate system are shown as u_g and v_g, respectively. Λ is a parameter related to the porosity in the soil, wherein $\Lambda = 1$ as $z \geqq z_b$, and $\Lambda = \lambda$ as $z < z_b$, where z_b is the bed level and λ is the porosity in the soil. Momentum equations of surface water are as follows:

$$\begin{aligned}
&\frac{\partial}{\partial t}\left(\frac{\mathrm{hU}}{J}\right) + \frac{\partial}{\partial \xi}\left(\frac{\mathrm{hUU}}{J}\right) + \frac{\partial}{\partial \eta}\left(\frac{\mathrm{hUV}}{J}\right) \\
&- \frac{\mathrm{hu}}{J}\left(U \frac{\partial}{\partial \xi}\left(\frac{\partial \xi}{\partial x}\right) + V \frac{\partial}{\partial \eta}\left(\frac{\partial \xi}{\partial x}\right)\right) \\
&- \frac{\mathrm{hv}}{J}\left(U \frac{\partial}{\partial \xi}\left(\frac{\partial \xi}{\partial y}\right) + V \frac{\partial}{\partial \eta}\left(\frac{\partial \xi}{\partial y}\right)\right) \\
&= -\mathrm{gh}\left(\frac{1}{J}\left(\left(\frac{\partial \xi}{\partial x}\right)^2 + \left(\frac{\partial \xi}{\partial y}\right)^2\right)\frac{\partial z}{\partial \xi}\right. \\
&\left. + \frac{1}{J}\left(\frac{\partial \xi}{\partial x}\frac{\partial \eta}{\partial x} + \frac{\partial \xi}{\partial y}\frac{\partial \eta}{\partial y}\right)\frac{\partial z_s}{\partial \eta}\right) - \frac{\tau_{b\xi}}{\rho J} \\
&+ \frac{1}{J}\left(\frac{\partial \xi}{\partial x}\right)^2 \frac{\partial}{\partial \xi}\left(h\sigma_{\mathrm{xx}}\right) + \frac{1}{J}\frac{\partial \xi}{\partial x}\frac{\partial \eta}{\partial x}\frac{\partial}{\partial \eta}\left(h\sigma_{\mathrm{xx}}\right) \\
&+ \frac{1}{J}\frac{\partial \xi}{\partial y}\frac{\partial \eta}{\partial x}\frac{\partial}{\partial \eta}\left(h\tau_{\mathrm{yx}}\right) + \frac{1}{J}\frac{\partial \xi}{\partial y}\frac{\partial \xi}{\partial x}\frac{\partial}{\partial \xi}\left(h\tau_{\mathrm{yx}}\right) \\
&+ \frac{1}{J}\frac{\partial \xi}{\partial x}\frac{\partial \eta}{\partial y}\frac{\partial}{\partial \eta}\left(h\tau_{\mathrm{xy}}\right) + \frac{1}{J}\frac{\partial \xi}{\partial x}\frac{\partial \xi}{\partial y}\frac{\partial}{\partial \xi}\left(h\tau_{\mathrm{xy}}\right) \\
&+ \frac{1}{J}\left(\frac{\partial \xi}{\partial y}\right)^2 \frac{\partial}{\partial \xi}\left(h\sigma_{\mathrm{yy}}\right) + \frac{1}{J}\frac{\partial \xi}{\partial y}\frac{\partial \eta}{\partial y}\frac{\partial}{\partial \eta}\left(h\sigma_{\mathrm{yy}}\right)
\end{aligned} \tag{7}$$

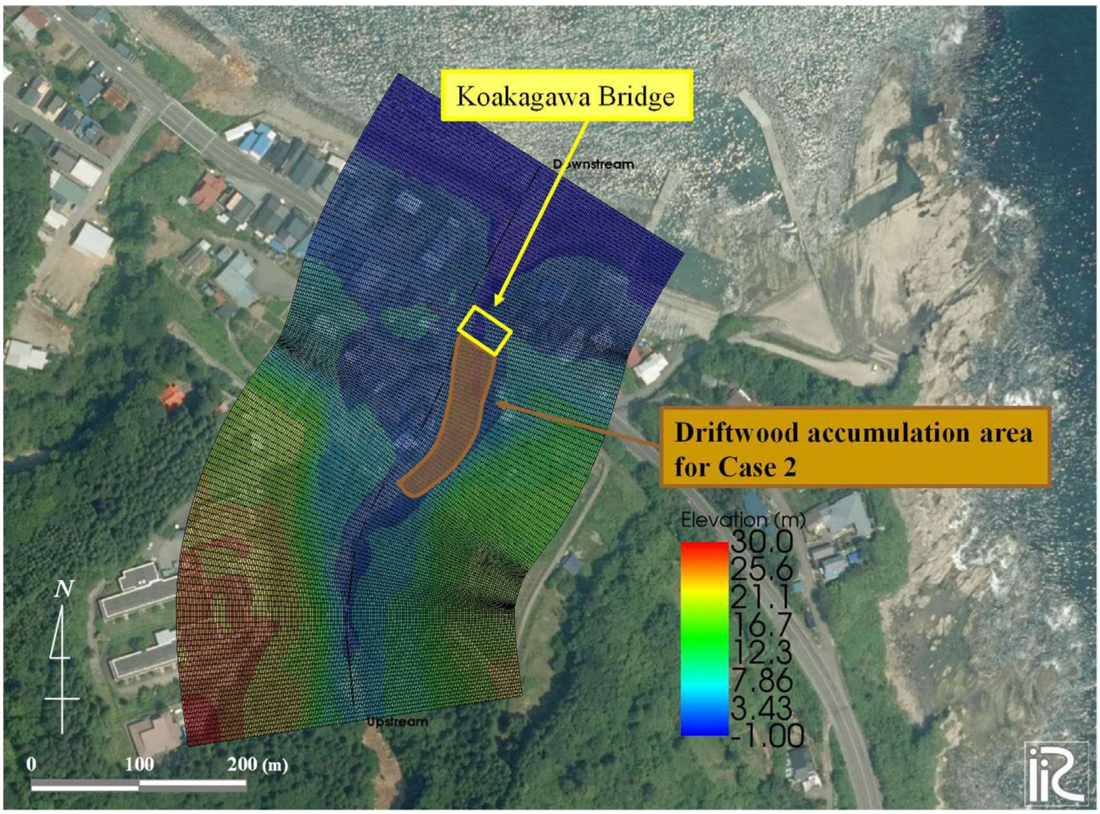

FIGURE 12 | Numerical analysis grids, land elevation, and driftwood accumulation area.

$$
\begin{aligned}
&\frac{\partial}{\partial t}\left(\frac{\mathrm{hV}}{J}\right)+\frac{\partial}{\partial \xi}\left(\frac{\mathrm{hVU}}{J}\right)+\frac{\partial}{\partial \eta}\left(\frac{\mathrm{hVV}}{J}\right)\\
&-\frac{\mathrm{hu}}{J}\left(U\frac{\partial}{\partial \xi}\left(\frac{\partial \eta}{\partial x}\right)+V\frac{\partial}{\partial \eta}\left(\frac{\partial \eta}{\partial x}\right)\right)\\
&-\frac{\mathrm{hv}}{J}\left(U\frac{\partial}{\partial \xi}\left(\frac{\partial \eta}{\partial y}\right)+V\frac{\partial}{\partial \eta}\left(\frac{\partial \eta}{\partial y}\right)\right)\\
&=-\mathrm{gh}\left(\frac{1}{J}\left(\frac{\partial \xi}{\partial x}\frac{\partial \eta}{\partial x}+\frac{\partial \xi}{\partial y}\frac{\partial \eta}{\partial y}\right)\frac{\partial z}{\partial \xi}\right.\\
&\left.+\frac{1}{J}\left(\left(\frac{\partial \eta}{\partial x}\right)^2+\left(\frac{\partial \eta}{\partial y}\right)^2\right)\frac{\partial z}{\partial \eta}\right)-\frac{\tau_{b\eta}}{\rho J}\\
&+\frac{1}{J}\frac{\partial \eta}{\partial x}\frac{\partial \xi}{\partial x}\frac{\partial}{\partial \xi}\left(h\sigma_{\mathrm{xx}}\right)+\frac{1}{J}\left(\frac{\partial \eta}{\partial x}\right)^2\frac{\partial}{\partial \eta}\left(h\sigma_{\mathrm{xx}}\right)\\
&+\frac{1}{J}\frac{\partial \eta}{\partial y}\frac{\partial \xi}{\partial x}\frac{\partial}{\partial \xi}\left(h\tau_{\mathrm{yx}}\right)+\frac{1}{J}\frac{\partial \eta}{\partial y}\frac{\partial \eta}{\partial x}\frac{\partial}{\partial \eta}\left(h\tau_{\mathrm{yx}}\right)\\
&+\frac{1}{J}\frac{\partial \eta}{\partial x}\frac{\partial \xi}{\partial y}\frac{\partial}{\partial \xi}\left(h\tau_{\mathrm{xy}}\right)+\frac{1}{J}\frac{\partial \eta}{\partial x}\frac{\partial \eta}{\partial y}\frac{\partial}{\partial \eta}\left(h\tau_{\mathrm{xy}}\right)\\
&+\frac{1}{J}\frac{\partial \eta}{\partial y}\frac{\partial \xi}{\partial y}\frac{\partial}{\partial \xi}\left(h\sigma_{\mathrm{yy}}\right)+\frac{1}{J}\left(\frac{\partial \eta}{\partial y}\right)^2\frac{\partial}{\partial \eta}\left(h\sigma_{\mathrm{yy}}\right)
\end{aligned}
\tag{8}
$$

where g is the acceleration due to gravity, and ρ is the water density. $\tau_{b\xi}$ and $\tau_{b\eta}$ represent the contravariant shear stress along the ξ and η coordinates, respectively. These shear stresses are defined as

$$\tau_{b\xi}=\frac{\partial \xi}{\partial x}\tau_{bx}+\frac{\partial \xi}{\partial y}\tau_{by} \tag{9}$$

$$\tau_{b\eta}=\frac{\partial \eta}{\partial x}\tau_{bx}+\frac{\partial \eta}{\partial y}\tau_{by} \tag{10}$$

where τ_{bx} and τ_{by} are the shear stresses along the x and y coordinates, respectively, and are given as follows:

$$\tau_{bx}=\tau_b\frac{u_b}{\sqrt{u_b^2+v_b^2}} \tag{11}$$

$$\tau_{by}=\tau_b\frac{v_b}{\sqrt{u_b^2+v_b^2}} \tag{12}$$

$$\frac{\tau_b}{\rho}=u_*^2 \tag{13}$$

$$u_*^2=\frac{n_m^2 g}{R^{1/3}}\left(u^2+v^2\right) \tag{14}$$

where u_* is the friction velocity, n_m is the Manning's roughness coefficient, and R is the hydraulic radius. u_b and v_b represent velocities near the bed surface along the x and y coordinates, respectively. Velocities near the bed are evaluated using the curvature radius of streamlines. σ_{xx}, σ_{yy}, τ_{xy}, and τ_{yx} are turbulence stresses. u_g and v_g represent velocities of seepage flow along the x and y coordinates, respectively, and are given as follows:

$$u_g=-k_{gx}\left(\frac{\partial \xi}{\partial x}\frac{\partial z}{\partial \xi}+\frac{\partial \eta}{\partial x}\frac{\partial z}{\partial \eta}\right) \tag{15}$$

$$v_g=-k_{gy}\left(\frac{\partial \xi}{\partial y}\frac{\partial z}{\partial \xi}+\frac{\partial \eta}{\partial y}\frac{\partial z}{\partial \eta}\right) \tag{16}$$

where k_{gx} and k_{gy} are the coefficients of permeability along the longitudinal and the transverse directions, respectively. When the water depth of surface flow becomes less than the mean diameter of the bed material, the surface flow is computed only in consideration of the pressure term and bed shear stress term in the momentum equation of surface flow.

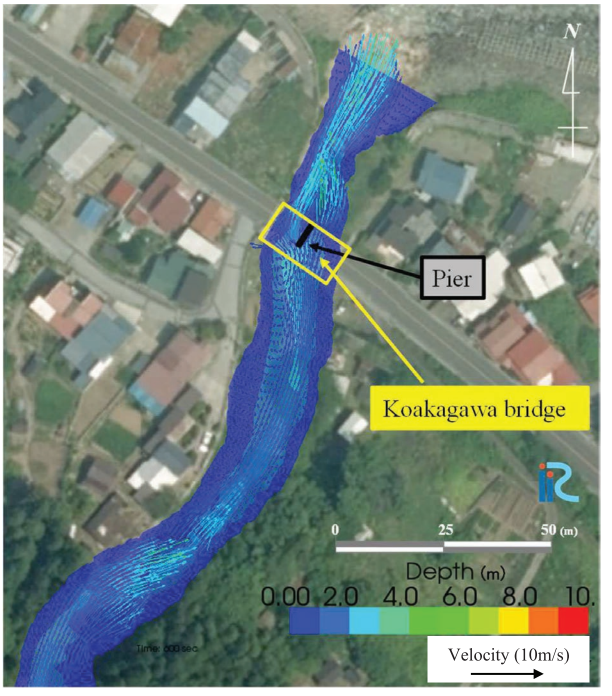

FIGURE 13 | Horizontal distribution of water depth and velocity vectors (Case 1).

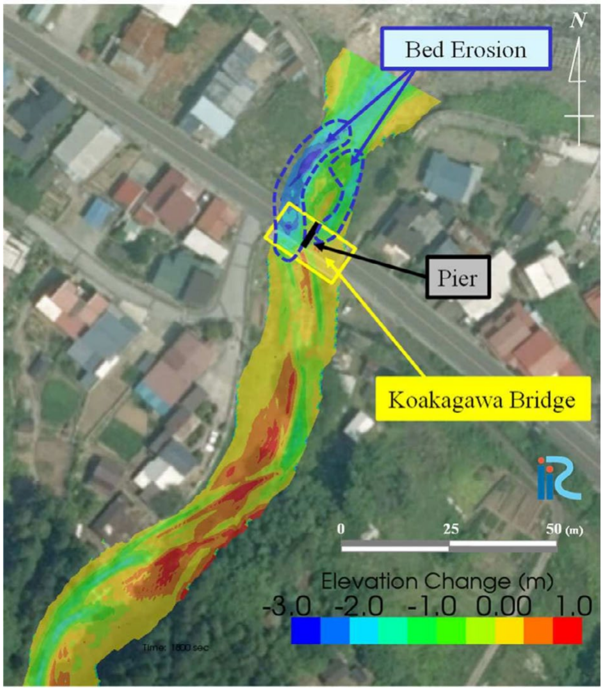

FIGURE 14 | Horizontal distribution of amount of bed deformation (Case 1).

The bed load is calculated using a modified Ashida–Michiue formula (Ashida and Michiue 1971; Kovacs and Parker 1994; Liu 1991). The effect of the local bed slope on the critical shear stress is considered.

The evolution of bed elevation is estimated using the following formula:

$$(1-\lambda)\frac{\partial}{\partial t}\left(\frac{z_b}{J}\right)+\left(\frac{\partial}{\partial \xi}\left(\frac{q_{b\xi}}{J}\right)+\frac{\partial}{\partial \eta}\left(\frac{q_{b\eta}}{J}\right)\right)=0 \tag{17}$$

where $q_{b\xi}$ and $q_{b\eta}$ are the bed load components in ξ and η directions. The local bed slope is reset to the angle of repose at calculation points where the slope becomes steeper than the angle of repose.

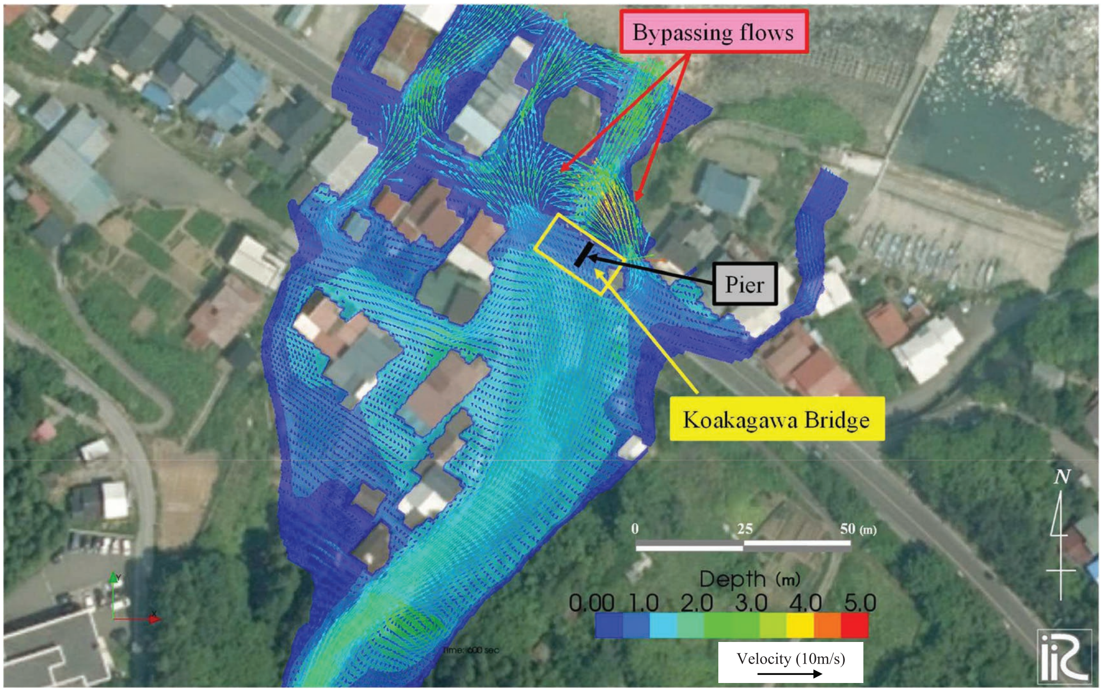

FIGURE 15 | Horizontal distribution of water depth and velocity vectors (Case 2).

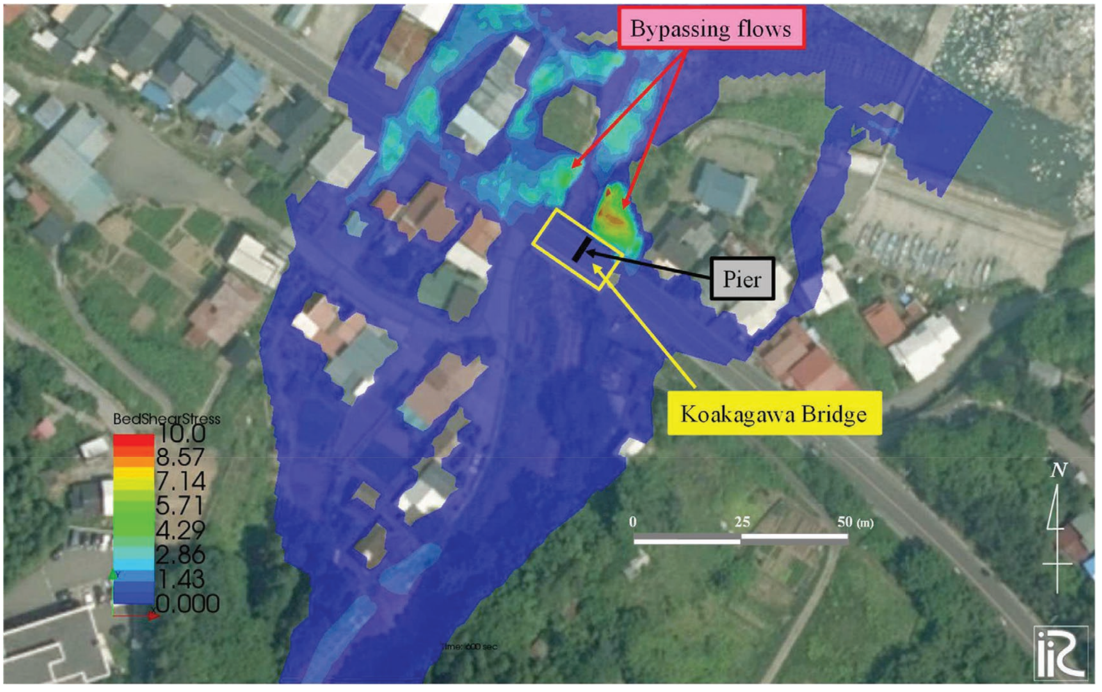

FIGURE 16 | Horizontal distribution of nondimensional shear stress (Case 2).

The continuum equation and the momentum equations for surface flow are discretized using the TVD-MacCormack scheme (Causon 1989).

3.2 | Hydraulic Conditions

Figure 12 shows the numerical analysis of grids and initial ground elevation used in the analysis. A 5 m DEM measured by the Geospatial Information Authority of Japan (GSI) was used as the initial ground elevation. The average numerical grid width was 1 m in the longitudinal direction and 0.5 m in the transverse direction, for a total grid number of 96,621 (301 in the longitudinal direction and 321 in the transverse direction). The average grain size of the bed material was 5 mm. Water was supplied at a rate of 26.5 m^3/s at steady state. Discharge was the peak flow discharge obtained by the rational equation using a runoff coefficient of 0.7, which was based on known values for heavy rainfall in the target mountain area, rainfall intensity of 30 mm/h, and a watershed area of 45,000 m^2. For rainfall intensity, the average of the mixed C- and X-band radar rainfall values from 2:00 to 7:00 on August 10 was used.

Based on photographs obtained after the disaster, as shown in Figure 5a, the maximum depth of the inundated water in the flooded area was less than 2 m, and the water surface level was lower than that of the roofs of one-story houses; therefore, the houses were treated as non-erodible obstacles. The pier of the Koakagawa Bridge is also treated as a non-erodible object.

Two cases were simulated: Case 1, in which driftwood was not considered, and Case 2, in which driftwood was considered. The accumulated driftwood area in Case 2 is indicated in Figure 12. After driftwood accumulated upstream of the Koakagawa Bridge, it was considered that the river was blocked by driftwood, and a small amount of water flowed through the driftwood accumulation area in the Koakagawa River. Therefore, the river channel in the driftwood accumulation area is filled with driftwood in the analysis, and the blown area in Figure 12 was treated as a non-erodible permeable body.

4 | Simulation Results and Discussion

Figure 13 shows the horizontal distributions of the water depth and velocity vectors for Case 1. The flood did not overflow from the Koakagawa River when there was no accumulation of driftwood upstream of the bridge. The flow was divided into right and left parts by the bridge pier as it passed the Koakagawa Bridge; the flow on the right side of the pier changed direction to the left bank just downstream of the Koakagawa Bridge, indicating that the flow was concentrated on the left bank downstream of the Koakagawa Bridge. Figure 14 shows the horizontal distribution of the amount of bed deformation after 1200 s in Case 1. It can be observed that the bed was eroded on both the left and the right sides of the bridge pier. In particular, the bed was deeply eroded on the left side of the pier and along the left bank downstream of the bridge. In this analysis, the pier was treated as a non-erosible object. Therefore, the erosion of the sediment beneath the pier could not be directly represented in this bed deformation analysis. However, the area around the piers was heavily eroded, as shown in Figure 14, and the bed material was not as cohesive, as shown in Figure 9. Therefore, it can be judged that the sediments under the piers were eroded along with the erosion of the sediments around the piers, causing the pier to sink, as shown in Figure 5b. Additionally, bed degradation along the left bank caused damage to the left bank revetment of the bridge.

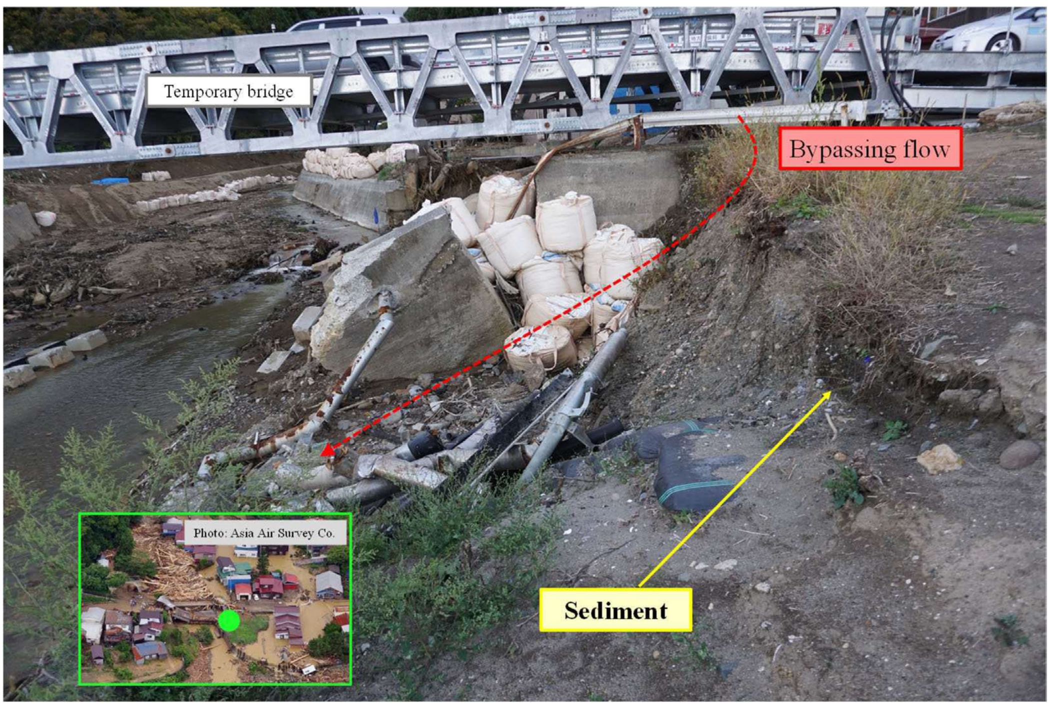

FIGURE 17 | Bank erosion around the bypassing flow on the left bank.

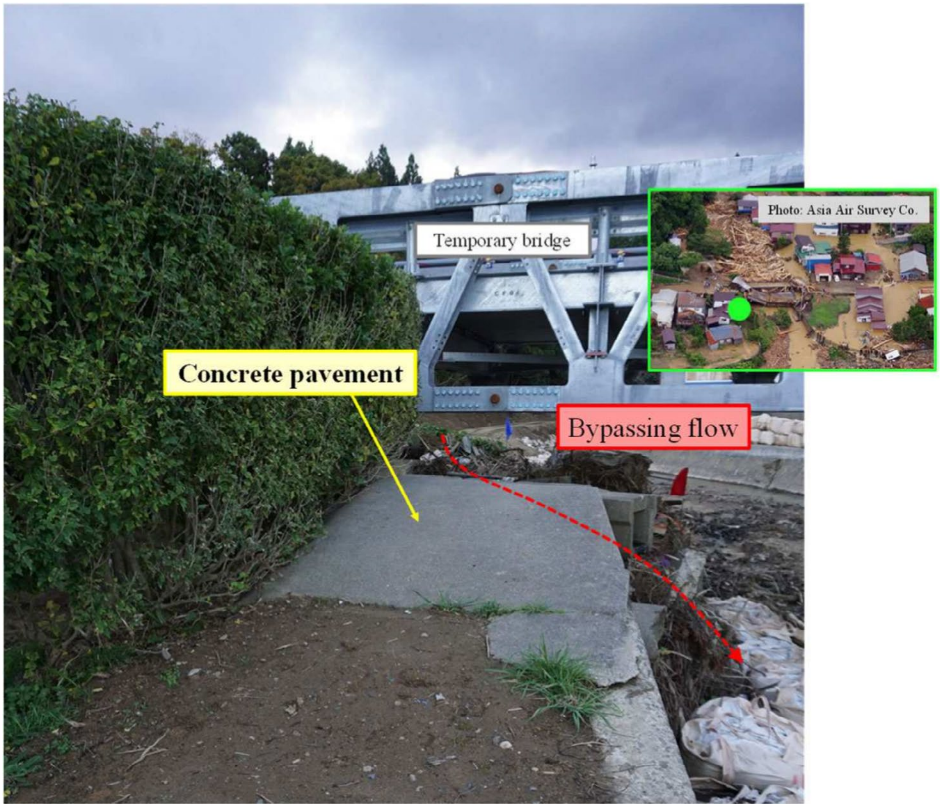

FIGURE 18 | Concrete pavement under the bypassing flow on the right bank.

Figure 15 shows the horizontal distributions of the water depth and velocity vectors for Case 2. As shown in the figure, the flood was attributed to the overflowing of the Koakagawa River due to channel blockage caused by driftwood. As indicated by the red arrows, bypassing flows, which are the flows of inundated water bypassing the bridge and returning to the river channel downstream, occurred on both the right and left banks of the Koakagawa Bridge, and bypassing flows from the right bank had a higher velocity. The bypassing flow flowed downstream of the bridge from the bank with higher ground into the riverbed with lower ground and resulted in rapid erosion of the bank (Wada et al. 2015). Figure 16 shows the horizontal distribution of the dimensionless shear stress. The dimensionless shear stress on the banks downstream of the Koakagawa Bridge was larger, thus indicating a flow condition in which the sediment discharge on the bank around the bridge can be large.

Figure 17 shows the left bank immediately downstream of the Koakagawa Bridge after the disaster. As shown in the figure, the left bank is heavily eroded because the ground surface on the left bank was composed of soil. The bypassing flow caused greater damage to the left bank side of the Koakagawa Bridge. These results indicate that the formation of bypassing flows caused by the accumulation of driftwood on the bridge was the cause of complete bridge failure. However, as shown in Figure 18, no bank erosion occurred on the right bank side, where the dimensionless shear stress was large, and the velocity of the bypassing flow was high. This is due to the fact that the ground on the right bank of the bridge, where the bypassing flow was formed, was covered with concrete, which suppressed ground erosion.

These results indicate that to prevent bank erosion caused by bypassing flows during floods, it is crucial to protect banks downstream of the bridge using non-erosive materials. A small area, where the non-dimensional shear stress exceeds the critical shear stress (e.g., 0.05) as shown in Figure 16, is sufficient for protection. Generally, river regulation work is carried out to prevent flood inundation, and the design of river structures considers only the external forces up to the water level at the top of the levee. Consequently, little is known about countermeasures for bypassing flows. However, to minimize damage from flood inundation, it is expected that bank erosion countermeasures against bypassing flows be implemented. Based on the results of field observation and numerical simulation presented here, the area of the bank to be protected is limited to a small area downstream of the bridge; thus, the cost of the countermeasure is not very high. Bypassing flows occur when the ground elevation of the floodplain is approximately the same as the top of the bank because the flood flow returns to the river channel downstream of the bridge. In other words, it occurs in a moated river channel rather than a constructed river channel. Additionally, because the blockage of the river channel by driftwood and sediment contributes to the occurrence of bypassing flows, countermeasures should only be taken on bridges located downstream of rivers where driftwood and sediment are predicted to be produced.

It is also important to predict bed degradation characteristics around a pier and banks. Bed degradation was rapid around the Koakagawa Bridge because the bed material is fine. Therefore, to prevent the subsidence of bridge piers, it is essential to implement sufficient erosion countermeasures (e.g., deep foundations) around bridge piers based on the predicted bed degradation.

Additionally, it is important to design the horizontal shape of the channel to ensure that water flow is not concentrated at the banks in the bridge cross-section, thereby avoiding the collapse of bridge revetment due to bed degradation along a bank.

5 | Conclusions

The cause of the collapse of the Koakagawa Bridge in Mutsu City, Aomori Prefecture, Japan, was investigated, along with the characteristics of flood inundation with bypassing flows and countermeasures for bank erosion due to channel blockage by driftwood. This investigation was based on field surveys and numerical simulations of horizontal two-dimensional bed deformation. It was determined that the initial collapse of the Koakagawa Bridge was caused by bed degradation around the bridge pier. The concentration of flow on the left bank of the river eroded the left bank, damaging the revetment. It was also concluded that flood inundation would not have occurred, even at peak flow discharge, if the channel had not been obstructed by driftwood. Additionally, the blockage of the channel by driftwood caused damage to the left bank and road through the formation of bypassing flows. However, the surface of the right bank, where the rapid bypassing flow formed, was covered with concrete; therefore, bank erosion did not occur on the right bank. These results indicate that to prevent bank erosion caused by bypassing flows during floods, it is important to protect banks downstream of the bridge using non-erosive materials. A small area where bypassing flows form and non-dimensional shear stress is larger than 0.05 is sufficient for this protection. Predicting bed degradation characteristics around piers and banks is also crucial. Bed degradation was rapid around the Koakagawa Bridge because the bed material was fine. Therefore, to prevent the subsidence of bridge piers, it is essential to implement sufficient erosion countermeasures around bridge piers based on the predicted bed degradation. Additionally, designing the horizontal shape of the channel to ensure that water flow is not concentrated at the banks in the bridge cross-section is important to avoid the collapse of bridge revetment due to bed degradation along the bank.

Acknowledgments

This work was funded by the Ministry of Land, Infrastructure, Transport and Tourism, Japan. The authors thank Aomori Prefecture and Kahoku Shimpo Publishing Co. for providing the information on the situation at the time of the disaster. The authors thank Asia Air Survey Co. Ltd. for providing the aerial photo used for this research.

Data Availability Statement

The datasets generated and/or analyzed during the current study are available from the corresponding author on reasonable request.

References

Ashida, K., and M. Michiue. 1971. "An Investigation of River Bed Degradation Downstream of a Dam." In *Proceedings of IAHR, 14th Congress*, 3, 247–255.

Bocchila, D., M. C. Rulli, and R. Rosso. 2006. "Transport of Large Woody Debris in the Presence of Obstacles." *Geomorphology* 76: 166–178.

Bocchila, D., M. C. Rulli, and R. Rosso. 2008. "A Flume Experiment on the Formation of Wood Jams in Rivers." *Water Resources Research* 44: W02408.

Bragg, D. C., and L. Kershner. 2004. "Sensitivity of a Riparian Large Woody Debris Recruitment Model to the Number of Contributing Banks and Tree Fall Pattern." *Western Journal of Applied Forestry* 19: 117–122.

Braudick, C. A., and G. E. Grant. 2001. "Transport and Deposition of Large Woody Debris in Streams: A Flume Experiment." *Geomorphology* 41: 263–283.

Braudrick, C. A., and G. E. Grant. 2000. "When Do Logs Move in Rivers?" *Water Resources Research* 36, no. 2: 571–583.

Causon, D. M. 1989. "High Resolution Finite Volume Schemes and Computational Aerodynamics, Nonlinear Hyperbolic Equation Theory, Computation Methods and Applications." *Notes on Numerical Fluid Mechanics* 24: 63–74.

Comiti, F., A. Lucía, and D. Rickenmann. 2016. "Large Wood Recruitment and Transport During Large Floods: A Review." *Geomorphology* 269: 23–39.

De Cicco, P. N., E. Paris, V. Ruiz-Villanueva, L. Solari, and M. Stoffel. 2018. "In-Channel Wood-Related Hazards at Bridges: A Review." *River Research and Applications* 34: 617–628.

Diehl, T. H. 1997. "Potential Drift Accumulation at Bridges." Publication No. FHWA-RD-97-028. US Department of Transportation, Federal Highway Administration Research and Development, Turner-Fairbank Highway Research Center: McLean, VA. http://www.tn.water.usgs.gov/pubs/FHWA-RD-97-028/drfront1.htm.

Fischer, M. 2006. "Driftwood During the Flooding in Klosters in (2005)." Report, HSW Wädenswil, Switzerland (in German). http://www.wsl.ch/fe/walddynamik/projekte/schwemmholzablagerungen/index_EN.

Igarashi, T., H. Takebayashi, H. Hamada, et al. 2016. "Development of Landslide and Debris Flow Disaster Information Distribution Service to Enhance Self-Evacuation." *Journal of Japan Society of Civil Engineers, Series B1 (Hydraulic Engineering)* 72, no. 4: I_1285–I_1290.

Köppen, W. 1936. *Das Geographische System Der Klimate*, 1–44. Gebrüder Borntraeger.

Kovacs, A., and G. Parker. 1994. "A New Vectorial Bedload Formulation and Its Application to the Time Evolution of Straight River Channels." *Journal of Fluid Mechanics* 267: 153–183.

Le Lay, Y.-F., and B. Moulin. 2007. "Dams and the Issue of Floating Wood: Gathering, Treating and Recovering." *La Houille Blanche-Revue Internationale De L Eau*, no. 3: 96–103. https://doi.org/10.1051/lhb:2007041.

Liu, B. Y. 1991. "Study on Sediment Transport and Bed Evolution in Compound Channels." Un-Published Doctoral Thesis Presented to Kyoto University.

Lucía, A., F. Comiti, M. Borga, M. Cavalli, and L. Marchi. 2015. "Dynamics of Large Wood During a Flash Flood in Two Mountain Catchments." *Natural Hazards and Earth System Sciences* 15: 1741–1755.

Lyn, D., T. Cooper, D. Condon, and L. Gan. 2007. "Factors in Debris Accumulation at Bridge Piers,Washington." US Department of Transportation, Federal Highway Administration Research and Development, Turner-Fairbank Highway Research Center, McLean, VA.

Lyn, D. A., T. Cooper, Y. K. Yi, R. Sinha, and A. R. Rao. 2003. "Debris Accumulation at Bridge Crossings: Laboratory and Field Studies." Paper Presented at Joint Transportation Research Program, Report No.: FHWA/IN/JTRP-2003/10, Purdue University, West Lafayette, IN, USA.

May, C. L., and R. E. Gresswell. 2003. "Large Wood Recruitment and Redistribution in Headwater Streams in the Southern Oregon Coast Range, U.S.A." *Canadian Journal of Forest Research* 33: 1352–1362.

Mazzorana, B., J. Hübl, A. M. Zischg, and A. Largiader. 2010. "Modelling Woody Material Transport and Deposition in Alpine Rivers." *Natural Hazards* 56, no. 2: 425–449.

Nelson, J. M., Y. Shimizu, T. Abe, et al. 2016. "The International River Interface Cooperative: Public Domain Flow and Morphodynamics Software for Education and Applications." *Advances in Water Resources* 93: 62–74.

Okamoto, T., H. Takebayashi, T. Kaneko, Y. Shibayama, and K. Toda. 2016. "Flood-Flow Characteristics in a Blocked River: Detour Flow Around a Bridge." In *Proceedings of Riverflow 2016 Congress*, St. Louis, 1869–1876.

Okamoto, T., H. Takebayashi, M. Sanjou, R. Suzuki, and K. Toda. 2020. "Log Jam Formation at Bridges and the Effect on Floodplain Flow: A Flume Experiment." *Journal of Flood Risk Management* 13, no. S1: e12562. https://doi.org/10.1111/jfr3.12562.

Panici, D., and G. A. de Almeida. 2018. "Formation, Growth, and Failure of Debris Jams at Bridge Piers." *Water Resources Research* 54, no. 9: 6226–6241.

Ruiz-Villanueva, V., E. Bladé, A. Díez-Herrero, J. Bodoque, and M. Sánchez-Juny. 2014. "Two-Dimensional Modelling of Large Wood Transport During Flash Floods." *Earth Surface Processes and Landforms* 39, no. 4: 438–449.

Ruiz-Villanueva, V., J. M. Bodoque, A. Díez-Herrero, and E. Bladé. 2014. "Large Wood Transport as Significant Influence on Flood Risk in a Mountain Village." *Natural Hazards* 74: 967–987.

Schalko, I. 2017. "Large Wood Accumulation Probability at a Single Bridge Pier." In Paper presented at the 37th IAHR World Congress, Kuala Lumpur, Malaysia, 1704–1713.

Schalko, I., L. Schmocker, V. Weitbrecht, and R. M. Boes. 2018. "Backwater Rise due to Large Wood Accumulations." *Journal of Hydraulic Engineering* 144, no. 9: 04018056.

Schmocker, L., and W. H. Hager. 2011. "Probability of Drift Blockage at Bridge Decks." *Journal of Hydraulic Engineering* 137: 470–479.

Schmocker, L., and W. H. Hager. 2013. "Scale Modeling of Wooden Debris Accumulation at a Debris Rack." *Journal of Hydraulic Engineering* 139: 827–836.

Takebayashi, H. 2017. "Braided Channels Under Unsteady Flow and the Effect of Spatiotemporal Change of Vegetation on Bed and Channel Geometry." In *Gravel-Bed River*, edited by D. Tsutsumi and J. B. Laronne. John Wiley & Sons Ltd. https://doi.org/10.1002/9781118971437.ch25.

Wada, T., H. Takebayashi, T. Kyuka, et al. 2015. "Flow and Bank Erosion Characteristics of Detour Flow Formed Around a Bridge." *Journal of Japan Society of Civil Engineers, Series B1 (Hydraulic Engineering)* 71, no. 4: I_895–I_900.

Wohl, E., and K. Jaeger. 2009. "A Conceptual Model for the Longitudinal Distribution of Wood in Mountain Streams." *Earth Surface Processes and Landforms* 34, no. 3: 329–344.